Numerical simulations of convection in Europa's ice shell: Implications for surface features

Adam P. Showman
Department of Planetary Sciences and Lunar and Planetary Laboratory, University of Arizona, Tucson, Arizona, USA

Lijie Han
Earth Sciences Division, Lawrence Berkeley National Laboratory, Berkeley, California, USA

Received 12 April 2003; revised 10 September 2003; accepted 1 December 2003; published 24 January 2004.

[1] Europa's icy surface displays numerous small (5- to 30-km-diameter) pits, spots, and uplifts that have been suggested to result from convection in the ice shell. To test this hypothesis, we present numerical simulations of convection in Europa's ice shell, including temperature-dependent viscosity and tidal heating. Ice shells 15 and 50 km thick are considered, consistent with several estimates of the shell thickness on Europa. The convection produces deep pits (consistent with some of the observed features) when the lithospheric viscosity is 10^3–10^5 times greater than that of the underlying ice, but greater viscosity contrasts lead to topography insufficient to explain the observed pits. If ductile creep is the only deformation mechanism, these results imply that convection cannot produce the observed pits and uplifts because in that case the predicted surface viscosity exceeds that of the warm underlying ice by at least a factor of 10^{10}. However, the strength of Europa's surface may be low enough for plastic deformation to play a role in the convection, opening the possibility that convection could produce some of Europa's pits. For plausible viscosities (10^{13} Pa s at the melting temperature), the pits are 100–300 m deep and 10–20 km in diameter; greater or lesser viscosities lead to wider or narrower pits, respectively. None of our simulations produced isolated uplifts of any diameter, however, so these probably formed by another mechanism. The convection can induce surface stresses >1 bar, which exceeds the inferred strength of Europa's crust and indicates the likelihood of surface disruption. The maximum tidal heat fluxes that can be transported by convection at realistic ice viscosities are 0.05–0.07 W m^{-2}. *INDEX TERMS:* 6218 Planetology: Solar System Objects: Jovian satellites; 5475 Planetology: Solid Surface Planets: Tectonics (8149); 5418 Planetology: Solid Surface Planets: Heat flow; 5430 Planetology: Solid Surface Planets: Interiors (8147); 8121 Tectonophysics: Dynamics, convection currents and mantle plumes; *KEYWORDS:* Europa, convection, tides, surface features, tectonics, geology

Citation: Showman, A. P., and L. Han (2004), Numerical simulations of convection in Europa's ice shell: Implications for surface features, *J. Geophys. Res.*, *109*, E01010, doi:10.1029/2003JE002103.

1. Introduction

[2] Europa's surface displays a diversity of geologic terrains. The two dominant terrain types are the ridged plains, which consist of successive generations of over-printed ridge pairs, and the chaos terrains, which are comprised of hummocky material and disrupted crustal blocks. In addition, numerous small (3- to 30-km-diameter) landforms were imaged by Galileo, including pits, domes, platforms, irregular uplifts, irregular lobate features, and disrupted "micro-chaos" regions (Figure 1) [*Pappalardo et al.*, 1998; *Greeley et al.*, 1998; *Greenberg et al.*, 2003; *Spaun et al.*, 1999; *Spaun*, 2002]. The topography of these features often reaches 100–300 m or more [*Greenberg et al.*, 2003; *Schenk and McKinnon*, 2001; *Schenk and Pappalardo*, 2002; *Figueredo et al.*, 2002]. Many of the depressions and uplifts alter the topography of the existing surface without disruption. Debate exists about the size distribution of the features; *Pappalardo et al.* [1998] argued from early analysis of Galileo images that a predominant diameter of ~10 km exists, which *Spaun* [2002] and *Spaun et al.* [1999] revised downward to ~4–6 km after an exhaustive survey of the complete image data set (which was not yet available to *Pappalardo et al.* [1998]). *Greenberg et al.* [2003] and *Riley et al.* [2000] also performed an exhaustive survey and argued that, when a preferred diameter exists at all, it is ~3 km and reflects the limits of resolution rather than a physical cutoff. In either case, however, the numerous observed features with diameters >3 km remain unexplained.

[3] Although several formation models exist for these features [*Greeley et al.*, 1998; *Greenberg et al.*, 1999; *Fagents et al.*, 2000], the most popular is that convection

0148-0227/04/2003JE002103$09.00

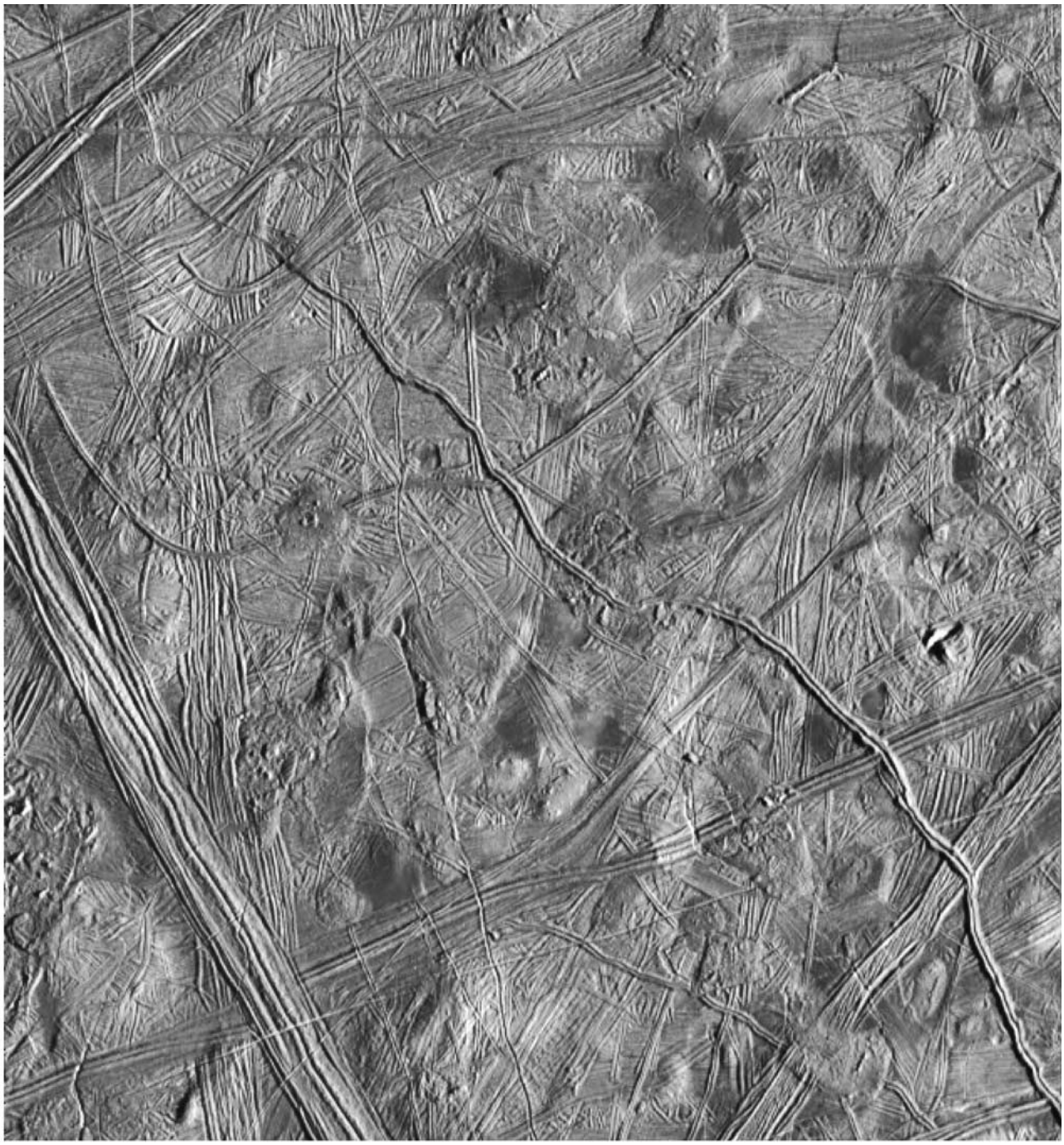

Figure 1. Regional Galileo image of Europa's surface near Conamara Chaos, showing numerous uplifts, pits, spots, and "micro-chaos" regions. The image spans about 140 by 130 km and is centered at latitude 12.3°N and longitude 268°W. Illumination is from the right.

in the underlying ice shell deforms the lithosphere, producing pits, domes, and disrupted regions [e.g., *Pappalardo et al.*, 1998; *Spaun*, 2002; *Head and Pappalardo*, 1999; *Collins et al.*, 2000; *Pappalardo and Head*, 2001; *Schenk and Pappalardo*, 2002; *Figueredo et al.*, 2002]. As yet, however, few quantitative studies investigating this hypothesis have been performed. Simplified calculations performed by *Nimmo and Manga* [2002] and *Rathbun et al.* [1998] suggested that small (2- to 3-km-diameter), coherent diapirs impinging against the lithosphere can produce domes of the inferred width, and *Nimmo and Manga* [2002] pointed out that if the diapirs formed at the base of the ice shell, then the lower thermal boundary layer thickness must be $\sim$1–2 km, which requires a relatively low ice viscosity of 10^{12}–10^{13} Pa s. But a full consideration of the convective dynamics (which was not undertaken by the above authors) is required to rigorously model diapir formation, evolution, and surface manifestation as a function of the background thermal state. Furthermore, rising diapirs are only one aspect of a complex overturning

Table 1. Model Parameters

Name	Symbol	Value
Acceleration of gravity	g	1.3 m s^{-1}
Density	ρ	917 kg m^{-3}
Thermal expansivity	α	$1.65 \times 10^{-4} K^{-1}$
Thermal diffusivity	κ	$1 \times 10^{-6} m^2$ s^{-1}
Temperature contrast	ΔT	175 K
Melting-temperature viscosity	η_0	primarily 10^{13} Pa s; 10^{12} and 10^{14} Pa s in a few runs
Thickness of ice shell	d	15 or 50 km

circulation, and a complete understanding of the relative roles of ascending and descending plumes in producing surface topography (as well as a self-consistent determination of the background thermal state itself) requires numerical simulations of the convection. It is therefore important to ascertain whether pits, uplifts, and disrupted micro-chaos regions result from a full numerical model of convection in Europa's ice shell. Several groups have begun to numerically model Europan convection [e.g., *Sotin et al.*, 2002; *Barr and Pappalardo*, 2003; *Tobie et al.*, 2002; *Wang and Stevenson*, 2000], but to date these studies have not emphasized the influence of the convection on surface topography.

[4] Here we present two-dimensional numerical simulations of solid-state convection in Europa's ice shell with the goal of determining implications for the surface features, especially the amplitude and wavelength of topography produced by the convection.

2. Model and Methods

[5] We used the ConMan finite-element code [*King et al.*, 1990] to solve the incompressible (Boussinesq) fluid equations neglecting inertia, as appropriate to a viscous, slowly convecting system. The simulations were performed in Cartesian (rectangular) geometry. In a convecting shell with a thickness comparable to the radius, spherical geometry would be required; however, Europa's ice-shell thickness is much less than Europa's radius, so rectangular geometry is sufficient.

[6] The code solves the dimensionless equations of momentum, continuity, and energy, respectively, given by

$$\frac{\partial \sigma_{ij}}{\partial x_j} + Ra\ \theta k_i = 0 \tag{1}$$

$$\frac{\partial u_i}{\partial x_i} = 0 \tag{2}$$

$$\frac{\partial \theta}{\partial t} + u_i \frac{\partial \theta}{\partial x_i} = \frac{\partial^2 \theta}{\partial x_i^2} + q' \tag{3}$$

where σ_{ij} is the dimensionless stress tensor, u_i is dimensionless velocity, θ is dimensionless temperature, q' is dimensionless heating rate, k_i is the vertical unit vector, t is dimensionless time, x_i and x_j are the dimensionless spatial coordinates, and i and j are the coordinate indices. Repeated spatial indices imply summation. For the development of the equations, see for example *Zhong and Gurnis* [1994a] or *Schubert et al.* [2001, chap. 6].

[7] The temperature dependence of the viscosity is contained in the constitutive relationship between stresses and strain rates, which, in dimensional form, is given by

$$\sigma_{ij} = -p\delta_{ij} + \eta\left(\frac{\partial u_i}{\partial x_j} + \frac{\partial u_j}{\partial x_i}\right) \tag{4}$$

where p is pressure, δ_{ij} is the Kronecker delta, and η is the temperature-dependent viscosity.

[8] The Rayleigh number Ra is given by

$$Ra = \frac{g\rho\alpha\Delta T d^3}{\kappa\eta_0} \tag{5}$$

where g is gravity, ρ is density, α is thermal expansivity, ΔT is the temperature drop between the bottom and top boundaries, d is the depth of the system, κ is the thermal diffusivity, and η_0 is the dynamic viscosity at the melting temperature. For reference, the model parameters are presented in Table 1.

[9] The velocity boundary conditions are periodic on the sides and free-slip rigid walls on the top and bottom. Because Europa's ice shell is underlain by a liquid-water ocean, the temperature at the base must remain at the melting temperature, and so we fix the bottom boundary to a temperature of 270 K. The top surface is maintained at 95 K, 35% of the basal temperature.

[10] The thickness of Europa's ice shell is a major unknown; we perform simulations primarily with thicknesses of 15 or 50 km, consistent with estimates of the ice-shell thickness from evolution, crater morphology, and crater size-distribution studies [*Hussmann et al.*, 2002; *Ojakangas and Stevenson*, 1989; *Turtle and Ivanov*, 2002; *Schenk*, 2002]. The ice-shell thickness in any given simulation remains constant throughout the simulation. The simulations were performed with aspect ratios (ratio of width to depth) ranging from 3 to 9.

[11] The adopted rheology is purely viscous, with a Newtonian, temperature-dependent viscosity. For the temperatures, stresses, and grain sizes that are likely in a convecting icy satellite, deformation by grain-boundary sliding (GBS) and diffusion are most relevant [*Goldsby and Kohlstedt*, 2001; *Durham and Stern*, 2001; *McKinnon*, 1998, 1999]. GBS is mildly non-Newtonian and grain-size sensitive, with a strain rate $\dot{\epsilon} \propto \sigma^{1.8} a^{-1.4}$, where σ and a are the stress and grain size, respectively [*Goldsby and Kohlstedt*, 2001]. Diffusion is Newtonian and leads to a strain rate $\dot{\epsilon} \propto \sigma a^{-2}$. The stresses and temperatures expected in the convecting region are probably 0.1–1 bar and 200–260 K [e.g., *McKinnon*, 1998], and while the grain sizes are unknown, estimates have suggested 0.1–1 mm [*Kirk and Stevenson*, 1987]. For constant grain size and temperature within the ranges given above, the rheological parameters given by *Goldsby and Kohlstedt* [2001] imply that the effective (stress-dependent) viscosity varies by only a factor of ~2–5 as stress is varied from 0.1–1 bar (depending on the relative importance of GBS and diffusion). This stress dependence is modest (for example, it is dwarfed by temperature variations in the viscosity, which are orders of magnitude) and suggests that to first order it is adequate to

approximate the viscosity as Newtonian. We therefore adopt a Newtonian temperature-dependent viscosity relevant for ice:

$$\eta = \eta_0 \exp\left[A\left(\frac{T_m}{T} - 1\right)\right] \quad (6)$$

where T is temperature, T_m is melting temperature, and η_0 is the viscosity at the melting temperature. Most of our simulations used $\eta_0 = 10^{13}$ Pa s, although we also explored 10^{12} and 10^{14} Pa s in a few cases. The value of A is maintained constant at 26, equivalent to an activation energy of 60 kJ mol^{-1} [see *Goldsby and Kohlstedt*, 2001].

[12] Simple prescriptions such as equation (6) imply that unfractured ice at Europa's 100-K surface temperature has a viscosity at least 10^{10} times that of the warm underlying ice, which, in absence of other effects, would preclude the surface layers from participating in the convection and lead to the formation of a stagnant lid at the surface [e.g., *Solomatov*, 1995; *Moresi and Solomatov*, 1995]. The fact that the ~10–30 bar failure strength of unfractured ice substantially exceeds the 0.1–1 bar convective stresses supports the idea that the surface remains immobile despite the existence of underlying convective motions. However, recent models for the formation of Europan cycloidal ridges imply that the fracture yield stress is only 0.4 bars [*Hoppa et al.*, 1999]. This implies that Europa's surface layer is extremely weak and raises the possibility that brittle deformation plays a role in the convection. On Earth, significant lithospheric deformation occurs along macroscopic faults and distributed microfractures from the surface to ~40 km depth [*Kohlstedt et al.*, 1995; *Tackley*, 2000a], and such deformation may be important in allowing plate tectonics [*Tackley*, 2000b]. The most appropriate way to incorporate such rheology is to allow plastic deformation when the shear stress exceeds a specified yield stress σ_Y (i.e., the viscosity would be that of equation (6) when the stress is less than σ_Y and would be $\sigma_Y/\dot{\epsilon}$, where $\dot{\epsilon}$ is the strain rate, when the stress exceeds σ_Y)[*Tackley*, 2000b]. However, such rheology allows complex nonlinear behavior, and for a first study of Europan convection, it is better to start with a simpler prescription that allows direct control of the effective viscosity associated with the plastic deformation. Accordingly, we parameterize the plastic behavior by terminating the increase in viscosity with decreasing temperature predicted by equation (6) when the viscosity exceeds a specified value that remains constant within a given simulation. The viscosity contrast χ, defined as the ratio between the maximum and minimum viscosities in the simulation, is a free parameter that we vary from 10^2–10^9. When equation (6) implies a local viscosity less than $\chi\eta_0$, that viscosity is used, but when the viscosity predicted by equation (6) exceeds $\chi\eta_0$ then the local viscosity is set equal to $\chi\eta_0$.

[13] Internal tidal heating is included in most simulations. Europa's tidal heating rate is poorly constrained and depends on the dissipation mechanisms and tidal flexing amplitude, which are not well known. *Ojakangas and Stevenson* [1989] pointed out that the Maxwell time of soft ice is comparable to Europa's tidal-flexing period, and they suggested that, because of this match, viscous creep may be the dominant contributor to tidal dissipation at tidal frequencies. Because of its simplicity, they and other authors have parameterized the dissipation using the Maxwell model, which yields a recipe in which the dissipation maximizes at a temperature near melting [e.g., *Ojakangas and Stevenson*, 1989; *Showman et al.*, 1997; *Hussmann et al.*, 2002; *Wang and Stevenson*, 2000; *Sotin et al.*, 2002; *Tobie et al.*, 2002]. One of the key implications is that the dissipation is greatest in the bottom part of the ice shell, where temperatures are warmest. However, alternative rheological models exist that would lead to different functional forms for the dissipation, and additional dissipation mechanisms may exist near melting and at very low temperatures, where the Maxwell model predicts small dissipation. In addition to these uncertainties, there is debate over how to extend the dissipation to multiple dimensions; some authors have suggested that the temperature dependence of tidal heating can cause runaway heating in hot upwelling plumes [*Sotin et al.*, 2002; *McKinnon*, 1999; *Wang and Stevenson*, 2000], but other authors argue that the tidal flexing, which causes the dissipation, cannot couple to small-scale convective structures [*Moore*, 2001]. Despite a lack of consensus on the details, most theoretical estimates place the average volumetric dissipation rate between 10^{-7} W m^{-3} and 3×10^{-6} W m^{-3} and the surface heat flux between ~0.01–0.1 W m^{-2} [*Hussmann et al.*, 2002; *Ojakangas and Stevenson*, 1989; *Ross and Schubert*, 1987].

[14] To span the range of possibilities, we run two sets of simulations. In the first set, we held the volumetric tidal heating rate q constant throughout the domain with a value between 10^{-7} and 10^{-5} W m^{-3} (some simulations were also performed with no tidal heating for comparison). This formulation gives us direct control over the heating magnitude so that we can easily quantify how the topography and background thermal state depend on the heating rate. In another set of simulations, q was determined by the Maxwell model, leading to a strong temperature dependence, with q maximizing at or near the melting temperature:

$$q = \frac{\epsilon_0^2 \omega^2 \eta}{2\left[1 + \frac{\omega^2 \eta^2}{\mu^2}\right]} \quad (7)$$

where $\omega = 2 \times 10^{-5}$ s^{-1} is Europa's tidal flexing frequency, $\mu = 4 \times 10^9$ Pa is the rigidity of ice, and ϵ_0 is the maximum magnitude of tidal flexing strain experienced by the ice shell during a tidal cycle. A crude estimate of ϵ_0 is simply ξ/R, where ξ is the amplitude of surface displacement during a tidal cycle and R = 1565 km is Europa's radius. For the expected internal structure (i.e., an ice shell, internal ocean, and silicate core), the vertical surface deformation during a tidal cycle is 20–30 m [*Moore and Schubert*, 2000; *Ross and Schubert*, 1987], implying $\epsilon_0 \sim 1$–2×10^{-5}. More detailed calculations confirm these values and show that for a mechanically uniform shell ϵ_0 varies spatially by a factor of about two, with minima near the equator and maxima near the poles [*Ojakangas and Stevenson*, 1989]. However, if Europa's ice shell is mechanically heterogeneous (for example, with much of the strain taken up within localized shear zones), then a wider range of values may be relevant. We vary ϵ_0 between 10^{-6} and 10^{-4}; within a given simulation, its value remains fixed in space and time.

[15] The normal stress at the top and bottom boundaries is non-zero and can vary spatially due to fluid-dynamical interactions; in a system with an open top surface, this would produce surface dynamic topography proportional to the normal stress. This fact has led to a standard prescription in the Earth mantle convection literature for calculating dynamic (i.e., convectively generated) topography [e.g., *Zhong and Gurnis*, 1994b], which we follow here. The dynamic topography is calculated from the relation

$$h = \frac{\sigma_{zz}}{\Delta\rho g} \tag{8}$$

where h is the dynamic topography, σ_{zz} is the (dimensional) vertical normal stress at the surface, $\Delta\rho$ is the density contrast across the interface (here equal to density itself), and g is gravity. This prescription is valid when h is much less than the wavelength of the topography, which is true here. The surface normal stress is calculated with the consistent boundary flux (CBF) method [see *Zhong et al.*, 1993].

[16] The simulation was initialized with a conductive temperature profile containing a weak perturbation near the bottom. The resolution was typically either 50 or 100 elements in the vertical direction and 150, 300, or 450 elements in the horizontal direction, depending on the aspect ratio of the simulation.

3. Results

[17] Consistent with analytical estimates [*McKinnon*, 1999], our simulations indicate that vigorous convection can occur in ice layers thicker than ~10–15 km, depending on the value of the melting-point viscosity η_0. The behavior of the convection and the resulting dynamic topography depend strongly on the viscosity contrast χ and also on the depth of the convecting system, melting-temperature viscosity η_0, and amplitude of internal heating q. We find that viscosity contrasts of 10^3–10^5 produce topography up to 100–300 m amplitude, whereas simulations with viscosity contrasts $\leq 10^2$ or $\geq 10^6$ generally have topography of ~30 m or less.

[18] When the viscosity contrast exceeds 10^6, the convective topography generally has characteristic wavelengths of 30–60 km (implying half-wavelength rises and valleys of 15–30 km width) and amplitudes of 30 m or less. This is illustrated in Figure 2, which depicts the temperature and dynamic topography for a simulation with a viscosity contrast of 10^9, layer thickness of 50 km, and melting-temperature viscosity of 10^{13} Pa s; essentially the same behavior is also observed for viscosity contrasts of 10^6, 10^7, and 10^8. Because of the temperature dependence of the viscosity, the convection is asymmetric, with a thick upper boundary layer, thin lower boundary layer, and a mean internal temperature in the convecting region that is about 97% of that at the base of the system. Numerous small-scale convective plumes, whose temperatures differ by <3% from that of their surroundings, rise from the base of the system and sink from the underside of the upper boundary layer. The viscosity near the top of the system is great enough to allow formation of a thick stagnant lid that does not participate in the convection [see *Solomatov*, 1995; *Moresi and Solomatov*, 1995]. Although warm rising plumes exist, they generally lose their coherency before they traverse the layer, and they have minimal topographic signature at the surface. Instead, the topography correlates with horizontal variations in the thickness of the stagnant lid, which is denser than the underlying material.

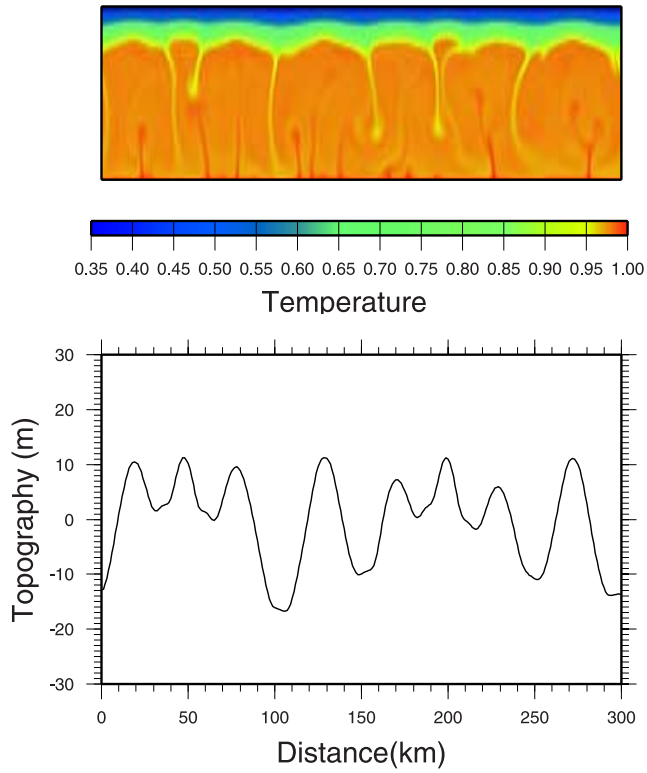

Figure 2. (top) Temperature divided by melting temperature for a simulation in a domain 300 km wide and 50 km deep. The viscosity contrast is 10^9, melting-temperature viscosity is 10^{13} Pa s, constant tidal heating is $q = 1 \times 10^{-7}$W m^{-3}, basal Rayleigh number is 4.3×10^8, and resolution is 300 × 50 in the horizontal and vertical directions. (bottom) Dynamic topography for the same simulation.

[19] When the viscosity contrast is 10^5 or less, the convective behavior changes drastically, leading to the production of deep, narrow depressions. Figures 3 and 4 show the temperature and dynamic topography resulting from simulations with a viscosity contrast of 10^4 and layer thicknesses of 50 km and 15 km, respectively. As before, numerous small-scale convective plumes, whose temperatures differ by <2% from that of their surroundings, rise from the base of the system and sink from the underside of the upper boundary layer. Furthermore, despite its stiffness, the upper boundary layer is mobile enough to descend in 10–20 km-wide downwellings whose temperatures are only 60–70% of that at the base of the system. This behavior indicates that the convection is in the transitional or "sluggish lid" regime described by *Solomatov* [1995]. Depressions 10–20 km wide and ≥100 m deep dominate the topographic expression. The depression widths are determined not by the depth of the convecting system but by the width of the downwellings, which underlie the depressions.

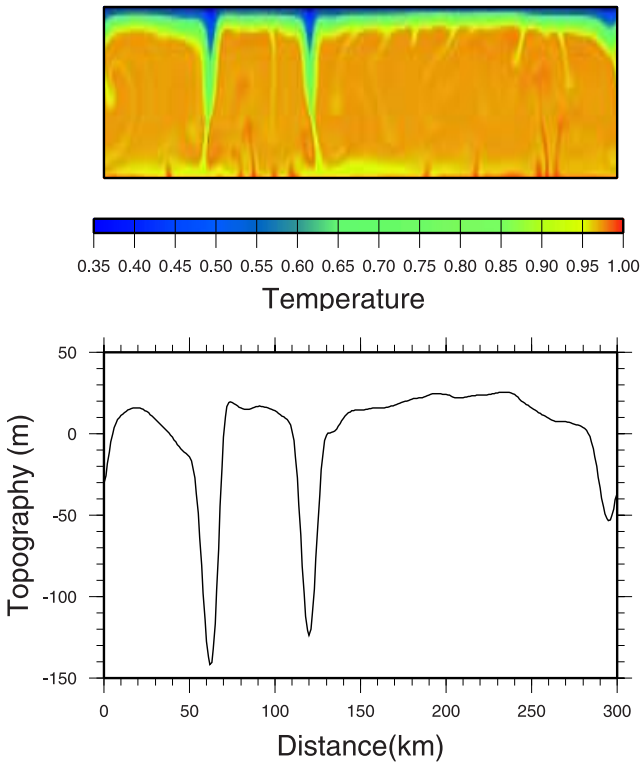

Figure 3. (top) Temperature divided by melting temperature for a simulation in a domain 300 km wide and 50 km deep. The melting-point viscosity η_0 is 10^{13} Pa s, viscosity contrast is 10^4, constant tidal heating rate is 3×10^{-7} W m^{-3}, basal Rayleigh number is 4.3×10^8, and resolution is 300 × 50 in the horizontal and vertical directions. (bottom) Dynamic topography for the same simulation.

Because dynamic topography results largely from horizontal buoyancy contrasts in the ice, it is the existence of the negatively buoyant descending plumes that causes the depressions.

[20] None of our simulations produce tall, isolated uplifts. This situation contrasts with conceptual [*Pappalardo et al.*, 1998] and analytical [*Nimmo and Manga*, 2002] models suggesting that positively buoyant diapirs can produce localized domes. In our simulations, the predominance of depressions and lack of domes occurs because the convective interior equilibrates at a temperature close to the melting temperature, which restricts the positive buoyancy of upwellings but allows great negative buoyancy in downwellings (if the viscosity contrast is low enough). A simple estimate illustrates this point. An isostatically adjusted column of height H with a temperature difference δT relative to the surroundings has a dynamic topography $h \sim H\alpha\delta T$, where $\alpha \sim 1.6 \times 10^{-4}$ K^{-1} is the thermal expansivity. The plumes ascending from the base are warmer than their environment by $\delta T \sim 0.02 T_m \sim 5$ K, implying that if they extend 20 km vertically, they would have dynamic topography of order 20 m. This is insufficient to explain the localized uplifts described by *Greenberg et al.* [2003], *Spaun* [2002], and *Pappalardo et al.* [1998]. Any partial melting within the ascending plume would counteract the plume's buoyancy, reducing the topography even more. In contrast, the descending plumes that underlie the depressions are $\sim 0.3 T_m \sim 80$ K colder than their surroundings, implying a topographic depression of amplitude $h \sim 260$ m for a plume extending 20 km vertically. Arguments similar to these explain why no deep depressions exist when the viscosity contrast $\geq 10^6$: because the coldest regions are immobile, the descending plumes have minimal buoyancy.

[21] We find that, as long as the system is in a convective state, the tidal heating has only a secondary effect on the dynamic topography, which (for $\chi \sim 10^3$–10^5) remains dominated by 100–300 m-deep depressions over a wide range of tidal heating rates. One could wonder whether reduced tidal heating would lead to cool enough temperatures in the convecting region for ascending plumes to produce tall domes (a result of their increased buoyancy relative to the cooler, denser background). However, simulations with no tidal heating do not produce domes; even in this case, the equilibrated temperature in the convecting region is $\sim 0.9 T_m$, which allows insufficient buoyancy in rising plumes for uplifts to be produced. Our simulations show tentative evidence that depressions are deeper when the tidal heating rate is lower, possibly because tidal heating in descending plumes lessens their negative buoyancy.

[22] All the simulations described so far were performed using a melting-point viscosity η_0 of 10^{13} Pa s. The

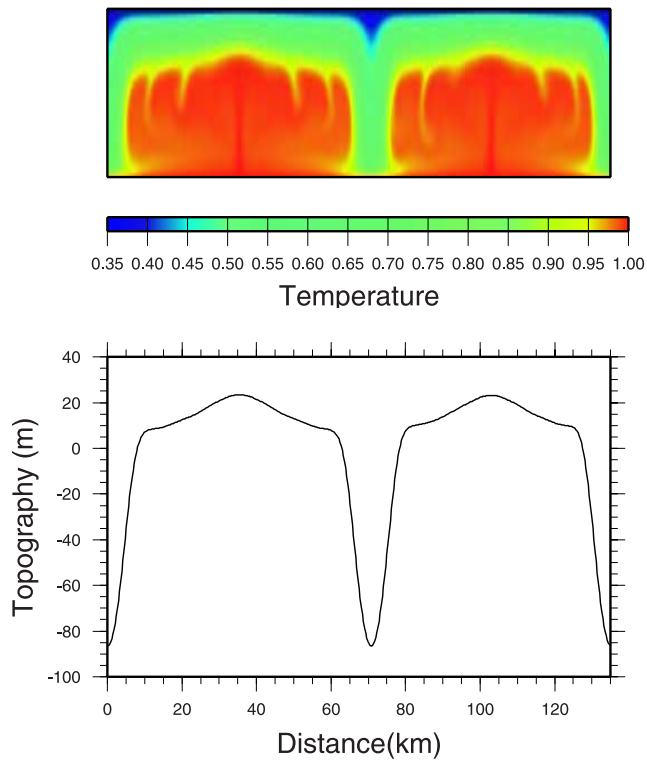

Figure 4. (top) Temperature divided by melting temperature for a simulation in a domain 135 km wide and 15 km deep. The melting-point viscosity η_0 is 10^{13} Pa s, viscosity contrast is 10^4, basal Rayleigh number is 1.2×10^7, and resolution is 450 × 50 in the horizontal and vertical directions. Tidal heating is temperature-dependent with tidal-flexing strain amplitude $\epsilon_0 = 2 \times 10^{-5}$. (bottom) Dynamic topography for the same simulation.

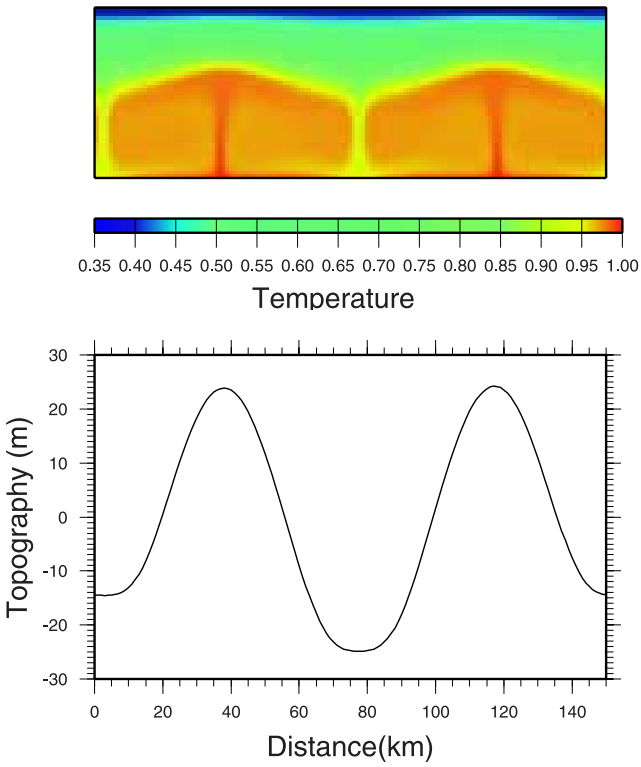

Figure 5. (top) Temperature divided by melting temperature for a simulation in a domain 150 km wide and 50 km deep with a melting-temperature viscosity of 10^{14} Pa s. The viscosity contrast is 10^8, tidal flexing amplitude $\epsilon_0 = 2 \times 10^{-6}$, basal Rayleigh number is 4.3×10^7, and resolution is 150×50. (bottom) Dynamic topography for the same simulation.

dependence of the convective behavior on η_0 is illustrated in Figures 5 and 6.

[23] Figure 5 shows the temperature and dynamic topography for a simulation with a melting-point viscosity of 10^{14} Pa s, layer thickness of 50 km (the same as in Figures 2 and 3), and viscosity contrast of 10^8. As in the high viscosity-contrast case shown in Figure 2, a thick stagnant lid forms, and the convective plumes underneath the lid have temperatures that deviate <3% from the mean temperature. The stiffer ice rheology leads to a steady-state convective pattern with cells 75 km wide and 25–30 km tall, which contrasts with the extreme time dependence of the convection in the higher Rayleigh number cases of Figures 2 and 3. The width of the convective cells is reflected in the dynamic topography, which, as in Figure 2, correlates with thickness variations in the stagnant lid.

[24] In contrast, Figure 6 illustrates the behavior for a simulation with $\eta_0 = 10^{12}$ Pa s, a layer thickness of 15 km (the same as in Figure 4), and a viscosity contrast of 10^4. As with the cases using this same viscosity contrast but stiffer melting-point viscosity (Figures 3 and 4), the cold ice near the top boundary in Figure 6 deforms sufficiently to descend in localized, extremely negatively buoyant downwellings (again indicative of the transitional or "sluggish lid" regime). The thin plumes that rise from the base, as in previous figures, have minimal buoyancy and often have insufficient vertical extent to impinge on the underside of the upper boundary layer. The key interesting feature is that the depressions are narrower than in previous figures; their diameters range from 7 to 20 km in this simulation.

[25] The extent to which the dynamic topography varies in time depends on the Rayleigh number. At basal Rayleigh numbers exceeding approximately 10^8 (depending on the viscosity contrast), the convection is highly time-dependent (see Figures 2, 3, and 6), and the topography undergoes order-unity variations on million-year timescales. In contrast, although the convection in Figure 4 exhibits some time-dependent characteristics (in particular the locations of the numerous thin, small-buoyancy plumes descending from the underside of the upper boundary layer), the basic convective planform and convective topography are steady in time. If the Rayleigh number is low enough, true steady-state behavior results (Figure 5). (The Rayleigh number below which the convection is steady and above which it is time-dependent increases with viscosity contrast. This explains why the convection in Figure 5 is steady and that in Figure 4 is marginally time-dependent despite the fact that the Rayleigh number in Figure 5 exceeds that in Figure 4 by a factor of nearly 4.) Any convectively generated topography on Europa could therefore exhibit either relatively steady or highly time-variable behavior, depending on the ice-shell thickness and viscosity.

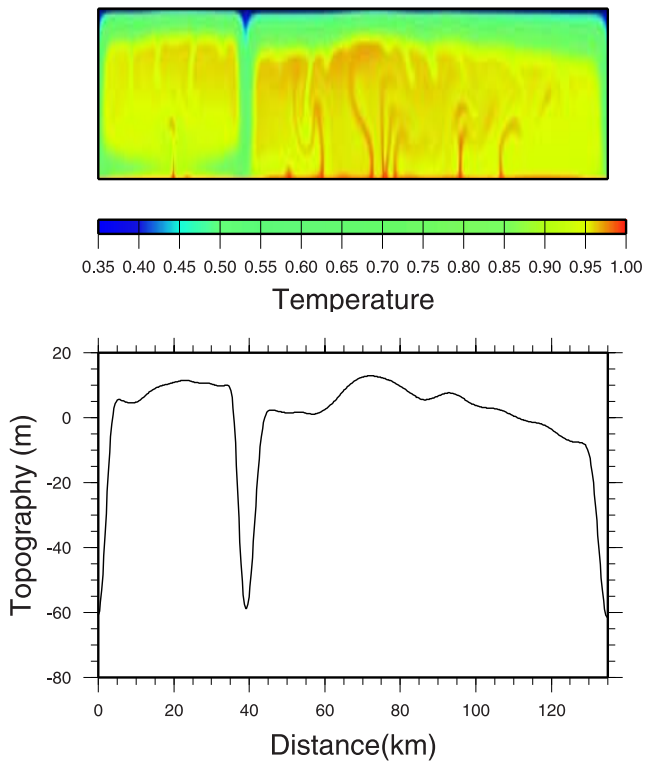

Figure 6. (top) Temperature divided by melting temperature for a simulation in a domain 135 km wide and 15 km deep with a melting-point viscosity of 10^{12} Pa s. The viscosity contrast is 10^4, constant tidal heating is $q = 1 \times 10^{-6}$W m^{-3}, basal Rayleigh number is 1.2×10^8, and resolution is 450×50 in the horizontal and vertical directions. (bottom) Dynamic topography for the same simulation.

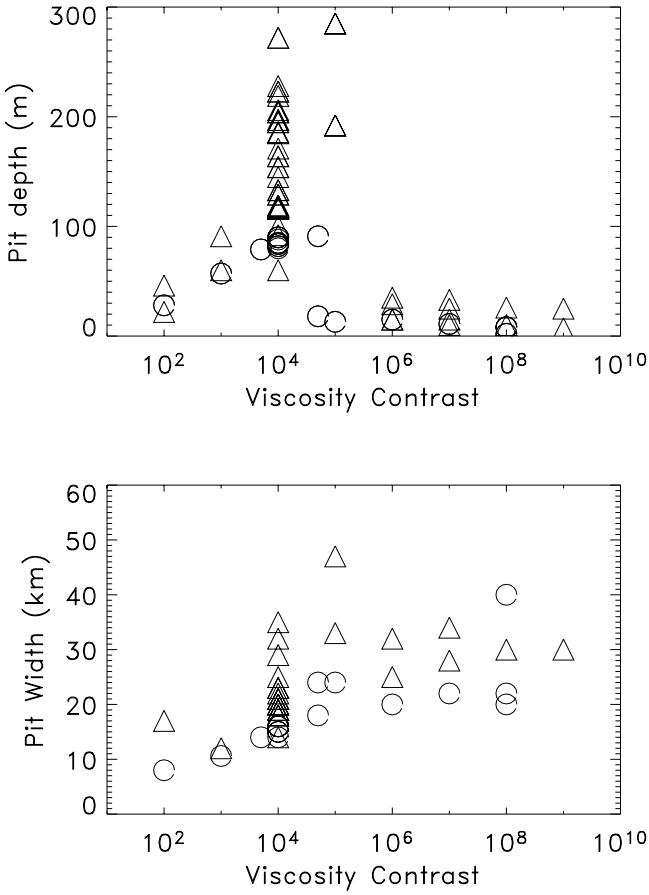

Figure 7. Summary of depth (top) and width (bottom) of pits produced by simulations with a melting-temperature viscosity of 10^{13} Pa s as a function of the viscosity contrast (i.e., the ratio between the maximum and minimum viscosities in the simulation). Circles and triangles denote simulations with depths of 15 and 50 km, respectively.

[26] It is important to realize that the dynamic topography exists because of the continued existence of convectively generated thermal anomalies, and if the convection ceased then the topography would disappear over $\sim 10^6$ years (the time for $\sim$10 km-wide thermal anomalies to diffuse away).

[27] Figure 7 summarizes the depths and widths of depressions as a function of viscosity contrast for a broad range of simulations performed using $\eta_0 = 10^{13}$ Pa s. The figure demonstrates that the pattern illustrated in Figures 2–4 holds generally: depression depths reach 100–300 m at viscosity contrasts of 10^3–10^5 but are <40 m at viscosity contrasts of 10^6 or more. The maximum depths of depressions for 50 km-thick layers, $\sim$300 m, is about three times greater than the $\sim$100-m maximum depth of depressions for 15-km-thick layers. This result is broadly consistent with the expectation that, for a given negative buoyancy in downwellings, dynamic topography h should scale with the depth of the layer H, i.e., $h \sim H\alpha\delta T$, where δT is the temperature difference between the downwelling and its surroundings. Furthermore, inspection of these simulations indicates that at viscosity contrasts $\leq 10^5$, the width of depressions is determined by the width of the downwelling plumes, whereas at viscosity contrasts $\geq 10^6$, topography instead tends to be associated with horizontal thickness variations of the stagnant lid. This fact helps explain the increase in depression widths with increasing viscosity contrast shown in Figure 7. Interestingly, when deep depressions exist, their diameters tend to be about three times greater than the thickness of the upper thermal boundary layer (as measured from the surface to the top of the adiabatic region).

[28] For the simulations we performed with constant tidal heating, the fact that ConMan solves the dimensionless equations allows us to rescale the existing simulations to infer the topography for cases with the same Rayleigh number but differing melting-point viscosities and ice-shell thicknesses. The output of a simulation constitutes the nondimensional temperatures, velocities, and stresses over a nondimensional domain as a function of nondimensional time for a specified Rayleigh number. The dimensional length, speed, time, tidal heating rate, and stress are then obtained by multiplying their nondimensional counterparts by d, κ/d, d^2/κ, $\Delta T\,\kappa\,\rho\,c_p/d^2$, and $\kappa\,\eta_0/d^2$, respectively. Here κ, ρ, c_p, and η_0 are the thermal diffusivity, density, specific heat, and melting-temperature viscosity; d is the depth of the system; and ΔT is the temperature difference between the bottom and top boundaries. (This rescaling cannot be performed for the simulations that used temperature-dependent tidal heating. Equation (7) implies that simulations with different melting-temperature viscosities should have different temperature dependences for the tidal heating, with the maximum in heating occurring at lower temperature in simulations with lower values of η_0. However, any given simulation with temperature-dependent heating has a specified temperature dependence, with the maximum in heating occurring at a particular temperature, and the rescaling cannot shift this temperature of maximum heating in the required manner. Therefore rescaling the simulations with temperature-dependent heating does not preserve the form of equation (7). This problem does not occur for the *constant* tidal-heating simulations, however, and we emphasize that the rescaling is fully rigorous for this case.) Suppose we want to rescale a simulation (say Figure 3) from $\eta_0 = 10^{13}$ Pa s to $\eta_0 = 10^{12}$ Pa s. For constant g, α, ρ, and ΔT (see equation (5)), maintaining constant Rayleigh number requires us to decrease d by a factor of $10^{1/3}$, or 2.15. The above relationships determine how the time, tidal heating rate, and stresses should be rescaled. As a result, Figure 3 also applies to a case with $\eta_0 = 10^{12}$ Pa s, d = 23.3 km, width of 139.5 km, and tidal heating rate of 1.38×10^{-6} W m^{-3}. The aspect ratio of the simulation is preserved during the rescaling, so the width of the simulation is reduced by the same factor as the depth. Instead of being $\sim$20 km wide, the depressions are thus 20 km/$10^{1/3} \approx 9$ km wide. The stresses should all be reduced by a factor of $10^{1/3}$, and the amplitude of the topography is reduced by the same factor (equation (8)). The 9-km-wide depressions are therefore $\sim$60 m deep.

[29] Applying this procedure to our simulations, we plot in Figure 8 the expected depth and width of depressions predicted by our simulations when they are rescaled to melting-point viscosities $\eta_0 = 10^{12}$ Pa s (left-hand axes) and 10^{14} Pa s (right-hand axes). Only simulations performed with constant tidal heating are included in this rescaling. Also plotted in Figure 8 are several simulations (including

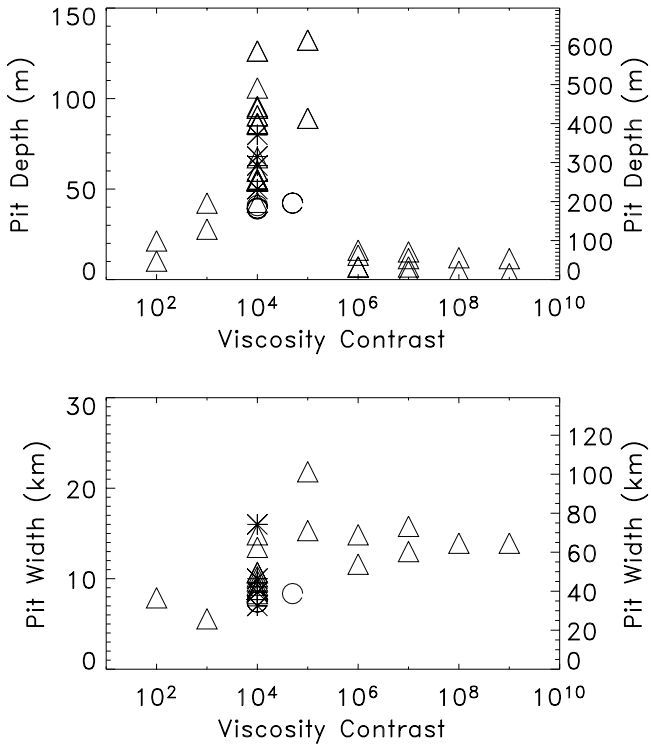

Figure 8. Depth (top) and width (bottom) of pits versus viscosity contrast in constant-heating simulations that have been rescaled to other melting-temperature viscosities. Left axes: Melting-temperature viscosity is 10^{12} Pa s; circles and triangles denote simulations with ice-shell thicknesses of 7 and 23.3 km, respectively. Right axes: Melting-temperature viscosity is 10^{14} Pa s; circles and triangles denote simulations with ice-shell thicknesses of 32 and 108 km, respectively. Asterisks denote 15-km-depth simulations conducted with $\eta_0 = 10^{12}$ Pa s (the left axes give their actual pit depths and widths; the right axes give their pit depths and widths when they are rescaled to $\eta_0 = 10^{14}$ Pa s, implying a rescaled depth d = 69.6 km).

that from Figure 6) explicitly conducted with $\eta_0 = 10^{12}$ Pa s and 15-km-thick shells. Their pit depths and widths overlap well with those from the rescaled simulations, illustrating the validity of the rescaling. And topographic amplitudes from the simulation in Figure 5, performed using $\eta_0 = 10^{14}$ Pa s, d = 50 km, and temperature-dependent tidal heating, also agree well with the constant-heating simulations shown in Figure 8 that were rescaled to $\eta_0 = 10^{14}$ Pa s.

[30] For the most realistic melting-temperature viscosities (10^{13}–10^{14} Pa s), topographic features generated by our simulations generally have diameters exceeding 10 km (Figures 7 and 8). This is problematic for the diapiric-origin hypothesis, because most pits, uplifts, and micro-chaos regions have diameters less than 6–8 km [*Spaun*, 2002; *Greenberg et al.*, 2003]. Melting-temperature viscosities of 10^{12} Pa s or less would allow convection to produce depressions with diameters <5 km (Figure 8), although this requires ice grain sizes less than 0.04 mm. It is also not clear whether such features would be as deep as observed Europan pits (200–300 m or more in some cases [*Greenberg et al.*, 2003; *Schenk and McKinnon*, 2001]). (Figure 8 hints that decreasing the viscosity lowers the stresses and makes the features shallower, but this may result from the fact that the rescaling requires us to reduce the ice-layer thickness when we reduce the viscosity. A full answer to this question will require thick-shell simulations with low viscosity, requiring basal Rayleigh numbers exceeding 10^9, and will be left for future work.) In summary, our simulations suggest that convection could produce some of Europa's widest depressions, but the numerous small (<5 km-diameter) depressions, and tall uplifts of any diameter, are difficult to explain.

[31] The spacing of deep depressions in our simulations ranges from 30 to 200 km, with values near ~100 km being most common, when the melting-temperature viscosity is 10^{13} Pa s. Increasing or decreasing the melting-temperature viscosity by an order of magnitude increases or decreases the spacing by a factor of two. In comparison, the observed spacing of uplifts and micro-chaos regions is 15–36 km [*Spaun et al.*, 2002; *Spaun*, 2002]. Therefore, as with the feature diameters, our simulations can only reproduce the typical observed spacing for extremely low viscosities ($\eta_0 \leq 10^{12}$ Pa s).

[32] In our simulations with a melting-point viscosity of 10^{13} Pa s, the maximum heat flux that can be supported by convection is ~0.05–0.07 W m^{-2}. Internal heat fluxes less than these values lead to equilibrated temperatures in the convective region that are less than the melting temperature. But tidal heating fluxes ≥0.05–0.07 W m^{-2} (corresponding to heating rates $\geq 1 \times 10^{-6}$ W m^{-3} and 5×10^{-6} W m^{-3} for 50 and 15 km-thick layers, respectively) cannot be convected out rapidly enough, and the temperature rises to the melting temperature. On Europa, this would cause widespread partial melting and lead to thinning of the ice shell. A rescaling similar to that previously described implies that for melting-temperature viscosities of 10^{12} and 10^{14} Pa s, the maximum fluxes consistent with a convecting ice shell are 0.11–0.15 W m^{-2} and 0.02–0.03 W m^{-2}, respectively.

4. Discussion

[33] We performed numerical simulations of convection in Europa's ice shell to test the hypothesis, suggested by numerous authors, that convection can produce Europa's pits and uplifts. Our simulations show that if the strength of Europa's near-surface ice is great enough for a stagnant lid to form at the surface (which occurs for viscosity contrasts $\geq 10^6$), then isolated pits or uplifts do not form. Instead, the convection produces smooth topographic swells that have amplitudes less than 40 m and wavelengths of typically 60 km. These topographic swells result from horizontal variations in the stagnant-lid thickness rather than diapiric activity; the internal density contrasts of the convecting interior are small enough that ascending and descending plumes have negligible influence on surface topography. However, we find that when the surface layers have viscosities only 10^3–10^5 times that of the underlying ice, the cold ice from 1–2 km depth is ductile enough to participate in the convection, leading to the production of deep depressions. For our standard cases with a melting-temperature viscosity of 10^{13} Pa s, the depressions are 100–300 m deep and ~10–20 km wide. These depths are similar

to pit depths observed on Europa, but the simulated diameters exceed that of most Europan pits. A rescaling of the results to other viscosities implies that the widths of the depressions are 5–15 km for a melting-temperature viscosity of 10^{12} Pa s and 20–60 km for a melting-temperature viscosity of 10^{14} Pa s. Therefore explaining the high abundance of pits with diameters ~5 km requires a melting-temperature viscosity of 10^{12} Pa s or less.

[34] On Europa, observational evidence suggests that the fracture yield stress at the surface is ~0.4 bar [*Hoppa et al.*, 1999]. Because Europan convective stresses can exceed 1 bar, it is therefore plausible that plastic deformation plays a role in the Europan convection. Terrestrial mantle-convection studies that include plastic rheology to account for lithospheric deformation indicate that the plastic behavior can lead, at least in some regions, to an effective viscosity contrast $\leq 10^5$ despite the fact that the viscosity contrast in absence of brittle effects should lie between 10^{40} and 10^{70}, and this behavior may be important in allowing plate tectonics [e.g., *Tackley*, 2000b]. On Europa, the exact viscosity contrasts that would result from a brittle lithospheric rheology remain to be seen, but it is plausible that they would be in the range ($\chi \sim 10^3$–10^5) that allows convectively generated topography.

[35] The fact that the convective stresses can exceed 1 bar, which is greater than the inferred strength of Europa's crust, indicates that surface disruption, and formation of chaos, could accompany the convection. The high surface stresses occur only near the deep depressions, so a correlation between convectively generated topography and chaos is predicted by our model.

[36] Even in the most generous cases, however, our simulations never produce uplifts or domes, only depressions. This results from the fact that the mean temperature in the convecting region equilibrates to at least 90% of the melting temperature, which strongly limits the positive buoyancy in ascending plumes. Furthermore, ascending plumes tend to be thin, less than 20 km tall, and often do not impinge on the underside of the stagnant lid (e.g., Figures 2 and 3), which further lessens their ability to produce a high-amplitude topographic signal at the surface. Interestingly, *Greenberg et al.* [2003] demonstrated in their analysis of Galileo images that the number density of Europan depressions exceeds that of uplifts, which is broadly consistent with our results.

[37] It is possible that Europa's uplifts result from compositional rather than thermal density contrasts, but this scenario has problems too. The most probable model of compositional diapirism is one wherein salt-free (hence low-density) diapirs ascend through a saltier, denser environment, but it is difficult to understand how such compositional gradients can be maintained against mixing if the shell is convecting. A thin, nonconvecting shell can maintain lateral compositional contrasts, but then the required density contrasts to produce Europan uplifts (which sometimes exceed 500 m in height) are implausibly large. Furthermore, any partial melting in the ice would tend to deplete the ice shell of salts (which percolate down into the ocean with the melt), so maintaining such compositional density contrasts is difficult. Domes might also result from cryovolcanism, either manifesting as surface deposits or subsurface intrusions [e.g., *Greeley et al.*, 1998; *Fagents et al.*, 2000; *Collins et al.*, 2000]. Long-term retention of the topography would require either lateral density contrasts in the ice or keels at the ice-ocean interface, which may be difficult to maintain over time; nevertheless, such alternatives deserve further study.

[38] Although convection can produce tall or deep isolated features only with difficulty, we have shown that it is easy for convection to produce broad, shallow topographic features. If Europa's ice shell is convecting, then numerous low-amplitude topographic undulations caused by the convection may exist across Europa's surface. Although such features are extremely hard to detect with current data, there are a few tantalizing possibilities. *Prockter and Pappalardo* [2000] documented the existence of a topographic undulation with 25-km wavelength and unknown amplitude, which they interpreted as compressive folds. Schenk and McKinnon [2001] also reported the existence of broad topographic swells tens of km across. Features such as these (including the superposed small-scale fractures and ridges described by Prockter and Pappalardo) may be consistent with a convective origin.

[39] The natural next step is to extend the simulations to three dimensions, which will allow better predictions for the geometry and spacing of topographic features. Other obvious improvements include adding non-Newtonian viscosity, allowing plastic deformation in the surface layers, and including the formation, advection, and percolation of partial melt. It would also be interesting to allow the thickness of the simulated shell to vary in response to freezing or melting and explore the extent to which the shell reaches a stable equilibrium rather than thinning or thickening over time.

[40] **Acknowledgments.** We thank A. Dombard, R. Greenberg, H. J. Melosh, F. Nimmo, P. Schenk, and P. J. Tackley for useful discussions.

References

Barr, A. C., and R. T. Pappalardo (2003), Numerical simulations of non-Newtonian convection in ice: Application to Europa, *Lunar Planet. Sci., XXXIV*, abstract 1477.

Collins, G. C., J. W. Head, R. T. Pappalardo, and N. A. Spaun (2000), Evaluation of models for the formation of chaotic terrain on Europa, *J. Geophys. Res.*, *105*, 1709–1716.

Durham, W. B., and L. A. Stern (2001), Rheological properties of water ice—Applications to satellites of the outer planets, *Annu. Rev. Earth Planet. Sci.*, *29*, 295–330.

Fagents, S. A., et al. (2000), Cryomagmatic mechanisms for the formation of Rhadamanthys Linea, triple band margins, and other low-albedo features on Europa, *Icarus*, *144*, 54–88.

Figueredo, P. H., F. C. Chuang, J. Rathbun, R. L. Kirk, and R. Greeley (2002), Geology and origin of Europa's "Mitten" feature (Murias Chaos), *J. Geophys. Res.*, *107*(E5), 5026, doi:10.1029/2001JE001591.

Goldsby, D. L., and D. L. Kohlstedt (2001), Superplastic deformation of ice: Experimental observations, *J. Geophys. Res.*, *106*, 11,017–11,030.

Greeley, R., et al. (1998), Europa: Initial Galileo geological observations, *Icarus*, *135*, 4–24.

Greenberg, R., et al. (1999), Chaos on Europa, *Icarus*, *141*, 263–286.

Greenberg, R., M. A. Leake, G. V. Hoppa, and B. R. Tufts (2003), Pits and uplifts on Europa, *Icarus*, *161*, 102–126.

Head, J. W., and R. T. Pappalardo (1999), Brine mobilization during lithospheric heating on Europa: Implications for formation of chaos terrain, lenticula texture, and color variations, *J. Geophys. Res.*, *104*, 27,143–27,155.

Hoppa, G. V., B. R. Tufts, R. Greenberg, and P. E. Geissler (1999), Formation of cycloidal features on Europa, *Science*, *285*, 1899–1902.

Hussmann, H., T. Spohn, and K. Wieczerkowski (2002), Thermal equilibrium states of Europa's ice shell: Implications for internal ocean thickness and surface heat flow, *Icarus*, *156*, 143–151.

King, S. D., A. Raefsky, and B. H. Hager (1990), ConMan: Vectorizing a finite element code for incompressible two-dimensional convection in the Earth's mantle, *Phys. Earth Planet. Inter.*, *59*, 195–207.
Kirk, R. L., and D. J. Stevenson (1987), Thermal evolution of a differentiated Ganymede and implications for surface features, *Icarus*, *69*, 91–134.
Kohlstedt, D. L., B. Evans, and S. J. Mackwell (1995), Strength of the lithosphere: Constraints imposed by laboratory experiments, *J. Geophys. Res.*, *100*, 17,587–17,602.
McKinnon, W. B. (1998), Geodynamics of icy satellites, in *Solar System Ices*, edited by B. Schmitt et al., pp. 525–550, Kluwer Acad., Norwell, Mass.
McKinnon, W. B. (1999), Convective instability in Europa's floating ice shell, *Geophys. Res. Lett.*, *26*, 951–954.
Moore, W. B. (2001), Coupling tidal dissipation and convection (abstract), *Bull. Am. Astron. Soc.*, *33*, 1107.
Moore, W. B., and G. Schubert (2000), The tidal response of Europa, *Icarus*, *147*, 317–319.
Moresi, L. N., and V. S. Solomatov (1995), Numerical simulations of 2D convection with extremely large viscosity variations, *Phys. Fluids*, *7*, 2154–2162.
Nimmo, F., and M. Manga (2002), Causes, characteristics and consequences of convective diapirism on Europa, *Geophys. Res. Lett.*, *29*(23), 2109, doi:10.1029/2002GL015754.
Ojakangas, G. W., and D. J. Stevenson (1989), Thermal state of an ice shell on Europa, *Icarus*, *81*, 220–241.
Pappalardo, R. T., and J. W. Head (2001), The thick-shell model of Europa's geology: Implications for crustal processes, *Lunar Planet. Sci.*, *XXXII*, abstract 1866.
Pappalardo, R. T., et al. (1998), Geological evidence for solid-state convection in Europa's ice shell, *Nature*, *391*, 365–368.
Prockter, L. M., and R. T. Pappalardo (2000), Folds on Europa: Implications for crustal cycling and accommodation of extension, *Science*, *289*, 941–943.
Rathbun, J. A., G. S. Musser, and S. W. Squyres (1998), Ice diapirs on Europa: Implications for liquid water, *Geophys. Res. Lett.*, *25*, 4157–4160.
Riley, J., G. V. Hoppa, R. Greenberg, B. R. Tufts, and P. Geissler (2000), Distribution of chaotic terrain on Europa, *J. Geophys. Res.*, *105*, 22,599–22,615.
Ross, M. N., and G. Schubert (1987), Tidal heating in an internal ocean model of Europa, *Nature*, *325*, 133–134.
Schenk, P. M. (2002), Thickness constraints on the icy shells of the Galilean satellites from a comparison of crater shapes, *Nature*, *417*, 419–421.
Schenk, P. M., and W. B. McKinnon (2001), Topographic variability on Europa from Galileo stereo images, *Lunar Planet. Sci.*, *XXXII*, abstract 2078.
Schenk, P. M., and R. T. Pappalardo (2002), Stereo and photoclinometric topography of chaos and anarchy on Europa: Evidence for diapiric origins, *Lunar Planet. Sci.*, *XXXIII*, abstract 2035.
Schubert, G., D. L. Turcotte, and P. Olson (2001), *Mantle Convection in the Earth and Planets*, Cambridge Univ. Press, New York.
Showman, A. P., D. J. Stevenson, and R. Malhotra (1997), Coupled orbital and thermal evolution of Ganymede, *Icarus*, *129*, 367–383.
Solomatov, V. S. (1995), Scaling of temperature- and stress-dependent viscosity convection, *Phys. Fluids*, *7*, 266–274.
Sotin, C., J. W. Head III, and G. Tobie (2002), Europa: Tidal heating of upwelling thermal plumes and the origin of lenticulae and chaos melting, *Geophys. Res. Lett.*, *29*(8), 1233, doi:10.1029/2001GL013844.
Spaun, N. A. (2002), Chaos, lenticulae, and lineae on Europa: Implications for geological history, crustal thickness, and the presence of an ocean, Ph.D. thesis, Brown Univ., Providence, R. I.
Spaun, N. A., et al. (1999), Spatial distribution of lenticulae and chaos on Europa, *Lunar Planet. Sci.*, *XXX*, abstract 1847.
Spaun, N. A., J. W. Head, and R. T. Pappalardo (2002), The spacing distances of chaos and lenticulae on Europa, *Lunar Planet. Sci.*, *XXXIII*, abstract 1723.
Tackley, P. J. (2000a), Mantle convection and plate tectonics: Toward an integrated physical and chemical theory, *Science*, *288*, 2002–2007.
Tackley, P. J. (2000b), Self-consistent generation of tectonic plates in time-depencent, three-dimensional mantle convection simulations: 1. Pseudo-plastic yielding, *Geochem. Geophys. Geosyst.*, *1*, Paper number 2000GC000036.
Tobie, G., G. Choblet, A. Mocquet, J. Pargamin, and C. Sotin (2002), Tidally heated convection within Europa's ice shell, *Lunar Planet. Sci.*, *XXXIII*, abstract 1498.
Turtle, E., and B. Ivanov (2002), Numerical simulations of crater excavation and collapse on Europa: Implications for ice thickness, *Lunar Planet. Sci.*, *XXXIII*, abstract 1431.
Wang, H., and D. J. Stevenson (2000), Convection and internal melting of Europa's ice shell, *Lunar Planet. Sci.*, *XXXI*, abstract 1293.
Zhong, S., and M. Gurnis (1994a), Role of plates and temperature-dependent viscosity in phase change dynamics, *J. Geophys. Res.*, *99*, 15,903–15,917.
Zhong, S., and M. Gurnis (1994b), Controls on trench topography from dynamic models of subducted slabs, *J. Geophys. Res.*, *99*, 15,683–15,695.
Zhong, S., M. Gurnis, and G. Hulbert (1993), Accurate determination of surface normal stress in viscous flow from a consistent boundary flux method, *Phys. Earth Planet. Inter.*, *78*, 1–8.

L. Han, Earth Sciences Division, Lawrence Berkeley National Laboratory, Mail Stop 90-1116, Berkeley, CA 94720, USA. (lhan@lbl.gov)
A. P. Showman, Department of Planetary Sciences and Lunar and Planetary Laboratory, University of Arizona, Tucson, AZ 85721, USA. (showman@lpl.arizona.edu)